Program Digest, 2019 IEEE International Ultrasonics Symposium (IUS)
Glasgow, Scotland, October 6-9, 2019

Integration of a CMUT linear array for wideband H-scan ultrasound imaging

Mawia Khairalseed [1,2], Kenneth Hoyt [1*]

Department of Bioengineering, University of Texas at Dallas, Richardson, TX, USA[1]
Department of Biomedical Engineering, Sudan University of Science and Technology and Africa City of Technology, Khartoum, Sudan [2]
[*] kenneth.hoyt@utdallas.edu

***Abstract*—A new modality has recently emerged for the ultrasound (US) classification of acoustic scatterers. Termed H-scan US, this imaging approach links the mathematics of Gaussian-weighted Hermite functions to the physics of scattering and reflection from different tissue structures within a standard convolutional model of pulse-echo US systems. The purpose of this study was to evaluate the use of a capacitive micromachined ultrasonic transducer (CMUT) for improved H-scan US imaging. Image data was acquired using a programmable US scanner (Vantage 256, Verasonics Inc) equipped with a 256-element L22-8v CMUT linear array transducer (Kolo Medical). Plane wave imaging was performed at a center frequency of 15 MHz. To generate the H-scan US image, three parallel convolution filters were applied to the radio frequency (RF) data to measure the relative strength of the received signals. After envelope detection, the relative strength of the filter outputs is color-coded to represent relative scatterer size. *In vitro* studies involved use of gelatin-based homogeneous phantoms that had different-sized spherical US scatterers, namely, 15, 30, or 45 µm. *In vivo* imaging of a breast tumor-bearing mouse was also used to test the new wideband H-scan US system. Results indicated that scatterers above 15 µm began to show good separation in the different Hermite. Findings from H-scan US imaging of a breast tumor–bearing mouse demonstrated that tumor tissue has a heterogenous distribution of scattering structures. Overall, H-scan US imaging is a promising approach for tissue classification and estimation of relative scatterer size.**

Keywords—angular compounding; CMUT; H-scan; plane waves; tissue characterization; ultrasound imaging

I. Introduction

The use of noninvasive ultrasound (US) for quantitative tissue characterization has been an exciting research prospect for several decades now. Herein the challenge is to find hidden patterns in the US data to reveal more information about tissue function and pathology that cannot be seen in the more conventional US images [1]. To that end, several different US-based tissue characterization methods have been introduced [2]–[10]. A limitation of some of these approaches is that they characterization accuracy, which can negatively impact spatial resolution and visualization of smaller tissue structures.

A new modality has recently emerged for pixel-level US classification of acoustic scatterers. Termed H-scan US imaging, this technique relies on matching a model of image formation to the mathematics of a class of Gaussian-weighted Hermite polynomial (GH) functions [11]. H-scan US is a simplified approach for detecting the frequency dependence of US scattering within different tissue types. In short, the backscattered US signal can be modeled as a convolution of an incident pulse with a sequence of tissue reflections [12]. Parallel convolution filters using GH of different orders are applied to the backscattered radio frequency (RF) US data to capture the relatively low and high frequency signal components, respectively. The resultant images are termed H-scan, where 'H' denotes Hermite (or hue for simplicity) to differ from the traditional B-scan US technique. H-scan US image intensity can be interpreted to describe different scattering structures or objects. In general, lower frequency spectral content is generated from larger scattering structures whereas higher frequency echo content is produced by an US wave interacting with small scatterers of scale below the wavelength of the US transmit pulse (i.e. Rayleigh scatterers). An overview of the H-scan concept was given in [13]–[19].

Compared to the traditional linear array piezoelectric transducers that were used with previous H-scan US imaging systems [13], [15], [16], [18], [19], a capacitive micromachined ultrasonic transducer (CMUT) have a higher sensitivity and significantly broader frequency response [20]. Therefore, CMUT technology is particularly attractive for wideband applications such as photoacoustic [21] or contrast-enhanced US [22] imaging. The purpose of this study was to evaluate the use of a CMUT linear array for improved H-scan US imaging.

II. Methodology

A. Ultrasound data acquisition

US data was acquired using a programmable US scanner (Vantage 256, Verasonics Inc, Kirkland, WA) equipped with a 256-element L22-8v CMUT linear array transducer (Kolo Medical Inc, San Jose, CA). Plane wave imaging was performed

This work was supported in part by National Institutes of Health (NIH) grants K25EB017222, R21CA212851, and R01EB025841 and Cancer Prevention Research Institute of Texas (CPRIT) award RP180670.

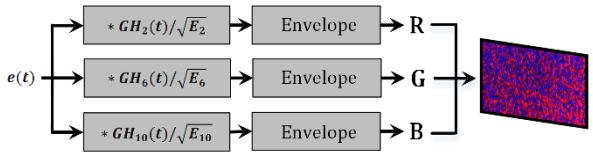

Fig. 1. Schematic diagram highlighting the parallel processing strategy used to generate and display an H-scan ultrasound (US) image. For a received US backscattered signal $e(t)$, convolution filtering with $GH_2(t), GH_6(t)$ and $GH_{10}(t)$ kernels are performed and assigned the red (R), green (G) and blue (B) channels of an RGB colormap, respectively, after envelope detection.

at a center frequency of 15 MHz on transmission and backscattered radio frequency (RF) data was sampled at a rate of 60 MHz and quantized at 12 bits. For spatial angular compounding, successively steered and overlapping plane wave transmissions were performed using five equally spaced angles in the ± 18° range [15]. The acoustic output was set to 1.1 MPa as measured using a hydrophone scanning system (AIMS III, Onda Corp, Sunnyvale, CA).

B. H-scan US Imaging

To generate the H-scan US image, three parallel convolution filters were applied to the RF data sequences to measure the relative strength of the received signals relative to $GH_2(t), GH_6(t)$ and $GH_{10}(t)$ after normalization by the signal energy $\sqrt{E_n}$. After envelope detection, the relative strength of the filter outputs is color coded whereby the lower frequency ($\mathbf{G}H_2 \cong 9$ MHz) backscattered US signal components are assigned to the R channel, moderate frequency ($\mathbf{G}H_6 \cong 15$ MHz) signals are assigned to the G channel, and the higher frequency ($\mathbf{G}H_{10} \cong 21$ MHz) signals to the B channel. This assignment completes the RGB color map and forms the H-scan US image. A schematic diagram summarizing the parallel processing and H-scan image display is presented in Fig. 1.

C. In vitro data

Testing of H-scan US imaging system functionality was conducted using a series of tissue-mimicking phantoms materials embedded with different-sized scatterers. Briefly, homogenous phantom materials were prepared by heating a 10% gelatin (300 Bloom, Sigma Aldrich, St. Louis, MO) in water solution to 45 °C. Silica microspheres (0.4% concentration, US Silica, Pacific, MO) were slowly introduced during constant stirring. The monodisperse silica microspheres were chosen to be either 15, 30, or 45 µm in diameter. All gelatin blocks were placed in a 4 °C refrigerator and allowed to cool for at least 12 h before use. Final phantom material sizes were about 12 cm × 12 cm × 8 cm (length × width × depth). H-scan US imaging of these homogeneous phantom materials (at room temperature, 25 °C) was then performed to detect the different-sized scattering objects and help optimize real-time H-scan US system imaging and control using the wideband CMUT linear array.

D. In vivo data

Animal experiments were reviewed and approved by the Institutional Animal Care and Use Committee (IACUC) at the University of Texas at Dallas. Briefly, human breast cancer cells (MDA-MB-231, ATCC, Manassas, VA) were maintained in Leibovitz's L-15 medium supplemented with 10% fetal bovine serum. All cells were cultured to approximately 90% confluence before passaging and grown at 37°C without CO_2 (Heracell 150i, Thermo Fisher Scientific, Waltham, MA, USA). Appropriate cell numbers were determined using a digital cell counting instrument (Countess II, Thermo Fisher Scientific).

Six-week-old female athymic mice (Charles River Laboratories, Wilmington, MA) were implanted orthotopically with 1 million breast cancer cells. Implanted tumors were allowed to grow for about three weeks before it was assessed using H-scan US imaging. During the US imaging study, animals were placed on a heating pad and controlled with 2% isoflurane anesthesia (Mobile Anesthesia Machine, Parkland Scientific, Coral Springs, FL).

E. Statistical analysis

All data was summarized as mean ± standard deviation. Statistical measures were computed from the weighted sum of the individual R, G, and B channel components.

III. Results and Discussions

A representative backscattered RF data segment and frequency content of the $GH_2(t)$, $GH_6(t)$ and $GH_{10}(t)$ filtering kernels are depicted in Fig. 2. While there is some correlation and spectral overlap of the GH kernels, they do successfully capture the broadband frequency signals encoded in the US data. These frequency bands are assumed to contain information on the different-sized scattering objects from small to large.

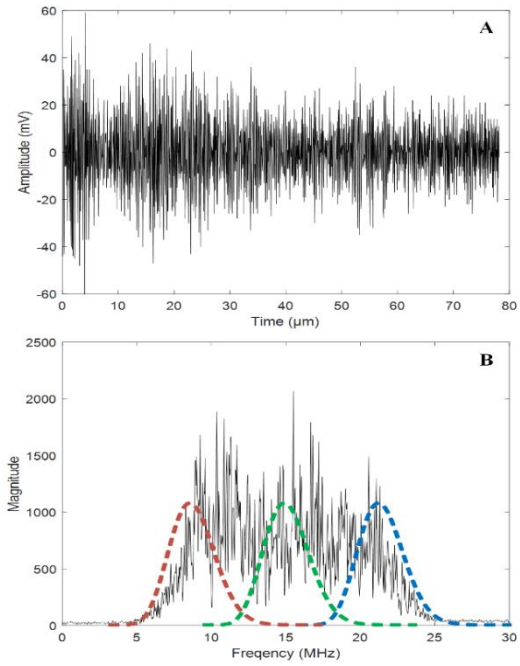

Fig. 2. (A) Segment of a backscattered US signal and corresponding (B) Frequency spectrum of this radio frequency (RF) data (black) and the three equally-spaced Gaussian-weighted Hermite polynomial (GWHP) bandpass filtering kernels.

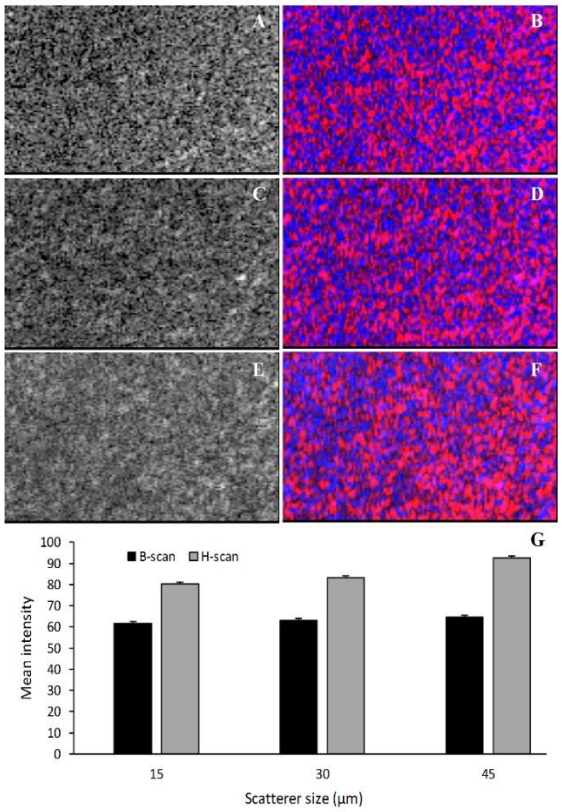

Fig. 3. Matched B-scan (left) and H-scan (right) US images of homogeneous tissue-mimicking test phantoms containing a mixture of different-sized spherical microparticles, namely, (A, B) 15, (C, D) 30, or (E, F) 45 μm-sized scatterers. (G) Mean B-scan and H-scan US image intensity measurements.

A series of soft tissue-mimicking phantom materials were used to test the new real-time H-scan US imaging system. Co-registered H-scan and B-scan US images were collected from phantoms with three distinctly different-sized (monodisperse) US scatterers, Fig. 3. Relative to image measurements from the phantom with 15 μm-sized scatterers, data from the phantom material with the 30 and 45 μm-sized scatterers exhibited mean H-scan US image intensity increases of 3.7% and 15.2%, respectively. Collectively, these findings indicate there is a progressive red color (hue) shift as the size of the acoustic scatterers are increased. This agrees with the H-scan US theory whereas larger scatterers dominate the red channel (low frequency spectrum). In comparison, the mean B-scan US image intensity increased by 2.5% and 5.0% for the phantom materials containing the 30 and 45 μm-sized scatterers, respectively. Since the backscattered US signal is proportional to the diameter of the scattering object, an increase in B-scan US image intensity is expected.

Using a 15 MHz center frequency from a transducer matching a $GH_6(t)$, the scatterers above 15 μm in diameter begin to show separation in the different Hermite filters. This fact helps explain why the mean H-scan US image intensity from phantom material containing the 15 μm scatterers relative to that with 30 μm scatterers had a lower change compared to that obtained from the phantom with the 45 μm scatterers.

A breast tumor–bearing mouse was imaged using the H-scan US system to estimate the relative size and spatial distribution of tissue structures, Figs. 4. Taking the ratio of the red to blue channel components throughout the tumor region, we found a mean ratio of 3.5. This finding indicates that the tumor had larger scattering structures (i.e. lower frequency signal) than smaller structures (i.e. higher frequency). Figs. 4 also illustrates tumor heterogeneity using a 3D histogram analysis, which summarize the number of occurrences (counts) in the H-scan US image as colored balls. Four histogram bins were selected for both the H-scan and B-scan US images. The H-scan US image had 32 distinct colors with each color ball representing different-sized tissue structures compared to only two groups in the B-scan US image using the same number of bins. This indicates a broader dynamic range for the H-scan US imaging technique and improved sensitivity to changes in scatterer size.

Distinguishing between different cells types and structures within a tumor can have significant implications for how cancers are diagnosed and treated. Existing approaches for testing tumor heterogeneity analyze excised tissue specimens but are limited because they contain a mixture of diverse cancer cell types and non-malignant cells [23]. Overall, H-scan US may represent a noninvasive imaging approach for detailing tumor tissue heterogeneity and likelihood of resistance to anticancer treatment. Future work should investigate physical size measurements at the cellular level correlated with H-scan US image features and cell variation over time (temporal heterogeneity). Also, we will develop new image formation strategies and colormap so all three channels (i.e. filter outputs) are better utilized.

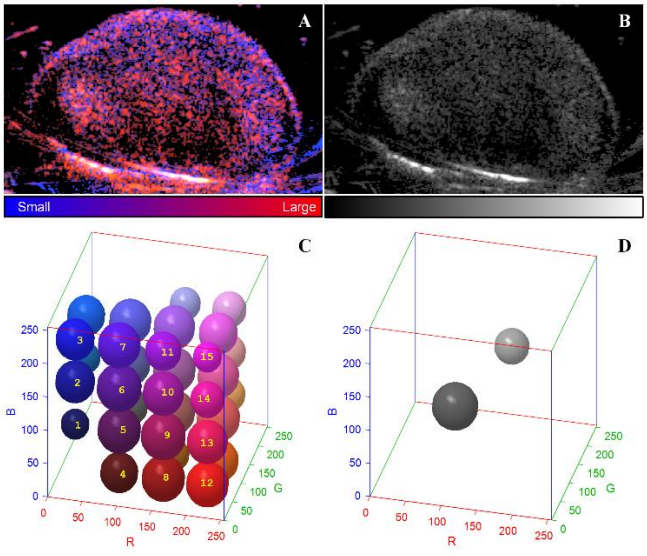

Fig. 4. Representative US results from a breast tumor-bearing animal. For comparison, both the (A) H-scan (B) B-scan US images are provided. Three-dimensional (3D) histogram analysis of the H-scan US image (C) reveals tumor tissue has a larger dynamic range compared to the (D) B-scan US image.

IV. Conclusions

H-scan is a new US-based imaging technique that locally estimates the relative size and spatial distribution of acoustic scattering objects and structures. As demonstrated, real-time and wideband H-scan US imaging can be implemented on a programmable US scanner and using angular compounded plane wave techniques. Results presented herein further suggests that high-resolution H-scan US imaging using a CMUT linear array is a promising modality for pixel-level tissue characterization.

References

[1] J. M. Thijssen, "Ultrasonic tissue characterisation and echographic imaging," *Physics in Medicine and Biology*, vol. 34, no. 11, pp. 1667–1674, 1989.

[2] J.-L. Gennisson, T. Deffieux, M. Fink, and M. Tanter, "Ultrasound elastography: principles and techniques," *Diagnostic and Interventional Imaging*, vol. 94, no. 5, pp. 487–495, 2013.

[3] M. C. Kolios, G. J. Czarnota, M. Lee, J. W. Hunt, and M. D. Sherar, "Ultrasonic spectral parameter characterization of apoptosis," *Ultrasound in Medicine & Biology*, vol. 28, no. 5, pp. 589–597, 2002.

[4] F. L. Lizzi, M. Astor, E. J. Feleppa, M. Shao, and A. Kalisz, "Statistical framework for ultrasonic spectral parameter imaging," *Ultrasound in Medicine & Biology*, vol. 23, no. 9, pp. 1371–1382, 1997.

[5] K. Hoyt, T. Kneezel, B. Castaneda, and K. J. Parker, "Quantitative sonoelastography for thein vivoassessment of skeletal muscle viscoelasticity," *Physics in Medicine and Biology*, vol. 53, no. 15, pp. 4063–4080, 2008.

[6] M. L. Oelze and W. D. O'Brien, "Method of improved scatterer size estimation and application to parametric imaging using ultrasound," *The Journal of the Acoustical Society of America*, vol. 112, no. 6, pp. 3053–3063, 2002.

[7] K. J. Parker, M. M. Doyley, and D. J. Rubens, "Imaging the elastic properties of tissue: the 20 year perspective," *Physics in Medicine and Biology*, vol. 56, no. 1, pp. R1–R29, 2010.

[8] C. S. Hall, E. D. Verdonk, S. A. Wickline, J. E. Perez, and J. G. Miller, "Anisotropy of the apparent frequency dependence of backscatter in formalin fixed human myocardium," *The Journal of the Acoustical Society of America*, vol. 101, no. 1, pp. 563–568, 1997.

[9] K. Hoyt, F. Forsberg, and J. Ophir, "Analysis of a hybrid spectral strain estimation technique in elastography," *Physics in Medicine and Biology*, vol. 51, no. 2, pp. 197–209, 2005.

[10] J. R. Doherty, G. E. Trahey, K. R. Nightingale, and M. L. Palmeri, "Acoustic radiation force elasticity imaging in diagnostic ultrasound," *IEEE Transactions on Ultrasonics, Ferroelectrics, and Frequency Control*, vol. 60, no. 4, pp. 685–701, 2013.

[11] A. D. Poularikas, *Transforms and applications handbook*, 3rd ed. CRC Press, 2018.

[12] T. L. Szabo, *Diagnostic ultrasound imaging: inside out*, 2nd ed., Boston: Academic Press, 2014.

[13] M Khairalseed, K Hoyt, J Ormachea, A Terrazas, and K. J. Parker, "H-scan sensitivity to scattering size," *Journal of Medical Imaging*, vol. 4, no. 4, pp. 1–7, 2017.

[14] M. Khairalseed, F. Xiong, R. Mattrey, K. Parker, and K. Hoyt, "Detection of early tumor response to abraxane using H-scan imaging: preliminary results in a small animal model of breast cancer," in *2017 IEEE International Ultrasonics Symposium (IUS)*, 2017, pp. 1–4.

[15] M. Khairalseed, F. Xiong, J.-W. Kim, R. F. Mattrey, K. J. Parker, and K. Hoyt, "Spatial angular compounding technique for H-scan ultrasound imaging," *Ultrasound in Medicine & Biology*, vol. 44, no. 1, pp. 267–277, 2018.

[16] M. Khairalseed, K. Brown, K. J. Parker, and K. Hoyt, "Real-time H-scan ultrasound imaging using a Verasonics research scanner," *Ultrasonics*, 2018.

[17] M. Khairalseed, K. Javed, G. Jashkaran, J.-W. Kim, K. J. Parker, and K. Hoyt, "Monitoring early breast cancer response to neoadjuvant therapy using H-scan ultrasound imaging: preliminary preclinical results," *Journal of Ultrasound in Medicine*, 2018.

[18] K. J. Parker, "Scattering and reflection identification in H-scan images," *Physics in Medicine and Biology*, vol. 61, no. 12, pp. L20–L28, 2016a.

[19] K. J. Parker, "The H-scan format for classification of ultrasound scattering," *OMICS Journal of Radiology*, vol. 05, no. 05, 2016b.

[20] Y. Huang *et al.*, "Comparison of conventional and collapsed region operation of capacitive micromachined ultrasonic transducers," *IEEE Transactions on Ultrasonics, Ferroelectrics, and Frequency Control*, vol. 53, no. 10, pp. 1918–1933, 2006.

[21] S. Vaithilingam *et al.*, "Three-dimensional photoacoustic imaging using a two-dimensional CMUT array," *IEEE Transactions on Ultrasonics, Ferroelectrics and Frequency Control*, vol. 56, no. 11, pp. 2411–2419, 2009.

[22] A. Novell, J.-M. Escoffre, and A. Bouakaz, "Second harmonic and subharmonic for non-linear wideband contrast imaging using a capacitive micromachined ultrasonic transducer array," *Ultrasound in Medicine & Biology*, vol. 39, no. 8, pp. 1500–1512, 2013.

[23] I. Dagogo-Jack and A. T. Shaw, "Tumour heterogeneity and resistance to cancer therapies," *Nature Reviews Clinical Oncology*, vol. 15, p. 81, 2017.